Original Article



Editor's Choice Investigation of the pharmacokinetic properties of synthetic heparan sulfate oligosaccharides

Katelyn Arnold¹, Zhangjie Wang¹, Andrew Lucas², William Zamboni², Yongmei Xu¹, Jian Liu^{1,*}

¹Division of Chemical Biology and Medicinal Chemistry, Eshelman School of Pharmacy, University of North Carolina, Chapel Hill, NC 27514, United States, ²UNC Advanced Translational Pharmacology and Analytical Chemistry (ATPAC) Laboratory, UNC Eshelman School of Pharmacy, UNC Lineberger Comprehensive Cancer Center, Carolina Institute of Nanomedicine, University of North Carolina, Chapel Hill, NC 27514, United States

*Corresponding author: Division of Chemical Biology and Medicinal Chemistry, UNC Eshelman School of Pharmacy120 Mason Farm Road, Genetic Medicine Building, Chapel Hill, NC 27514, United States. Email: jian liu@unc.edu

Heparan sulfate (HS) is a sulfated polysaccharide with a wide range of biological activities. There is an increasing interest in the development of structurally homogeneous HS oligosaccharides as therapeutics. However, the factors influencing the pharmacokinetic properties of HS-based therapeutics remain unknown. Here, we report the pharmacokinetic properties of a panel of dodecasaccharides (12-mers) with varying sulfation patterns in healthy mice and uncover the pharmacokinetic properties of an octadecasaccharide (18-mer) in acutely injured mice. In the 12-mer panel, 1 12-mer, known as dekaparin, is anticoagulant, and 3 12-mers are nonanticoagulant. The concentrations of 12-mers in plasma and urine were determined by the disaccharide analysis using liquid chromatography coupled with tandem mass spectrometry. We observed a striking difference between anticoagulant and nonanticoagulant oligosaccharides in the 12-mer panel, showing that anticoagulant dekaparin had a 4.6-fold to 8.6-fold slower clearance and 4.4-fold to 8-fold higher plasma exposure compared to nonanticoagulant 12-mers. We also observed that the clearance of HS oligosaccharides is impacted by disease. Using an antiinflammatory 18-mer, we discovered that the clearance of 18-mer is reduced 2.8-fold in a liver failure mouse model compared to healthy mice. Our results suggest that oligosaccharides are rapidly cleared renally if they have low interaction with circulating proteins. We observed that the clearance rate of oligosaccharides is inversely associated with the degree of binding to target proteins, which can vary in response to pathophysiological conditions. Our findings uncover a contributing factor for the plasma and renal clearance of oligosaccharides which will aid the development of HS-based therapeutics.

Key words: heparan sulfate; pharmacokinetics; synthetic oligosaccharide; therapeutics.

Introduction

Heparan sulfate (HS) is a sulfated polysaccharide that is abundant on the cell surface and in the extracellular matrix. Heparin is a commonly used anticoagulant drug and is a highly sulfated form of HS. Heparin drugs include unfractionated heparin (UFH), low molecular weight heparin (LMWH), and fondaparinux(Oduah et al. 2016). Interestingly, the structure of UFH and LMWH can be modified to remove anticoagulant activity by selective desulfation (Fryer et al. 1991) or oxidative cleavage, resulting nonanticoagulant heparin (Ouyang et al. 2019). There is considerable interest in the pharmacological activities of nonanticoagulant heparin in diseases like cancer (Mohamed and Coombe 2017), cystic fibrosis (Voynow et al. 2020), and viral infection (Clausen et al. 2020). However, clinical development of nonanticoagulant heparin is difficult due to the heterogenous composition. For example, defining the pharmacokinetics relies on measuring the pharmacodynamic effect. Pharmacokinetics of anticoagulant heparin drugs are measured indirectly using a chromogenic FXa activity assay (Baglin et al. 2006). Drug concentration is correlated with activity rather than detecting the drug molecules. However, for nonanticoagulant heparin, there is no equivalent method for measuring activity, which presents a challenge for pharmacokinetic analysis of these saccharides.

Measuring intact nonanticoagulant heparin can be achieved by using radioactively labeled compounds, but the application is limited to animal studies. A recent study proposed the use of a commercially available Heparin Red kit for the detection of nonanticoagulant heparin (Warttinger et al. 2016). This method relies on the chain length and negative charge of heparin polysaccharides to quench a fluorescent probe. Because of these detection requirements, the Heparin Red method is most sensitive for UFH detection and has decreased responsiveness to shorter and less sulfated polysaccharides compared to UFH. Here, we present a significant advancement in the detection of anticoagulant and nonanticoagulant oligosaccharides in biological matrixes. Our detection method directly measures the disaccharide building blocks in heparin and HS and does not rely on the anticoagulant activity, overall negative charge, or size. The liquid chromatography coupled with tandem mass spectrometry (LC-MS/MS) and ¹³C-labeled calibrants allowed for quantitative, sensitive analysis(Wang et al. 2020). In this manuscript, we carry out the pharmacokinetic analysis of 4 structurally defined 12mers and 1 18-mer in both healthy mice and acute liver injury mouse model. Our results show that anticoagulant and nonanticoagulant oligosaccharides have dramatic pharmacokinetic differences. Binding to target proteins increases the oligosaccharide plasma area under the concentration curve (AUC). This principal is further demonstrated with 18-mer in the acute liver injury model where the target protein is released into circulation and AUC increased. These results are essential for future therapeutic oligosaccharide development efforts. As an example, based on the PK results, we modified our dosing

regimen in the acute liver injury model. We achieved a greater liver protection with the modified dose regimen. This method for detecting and quantifying concentration will be necessary to advance nonanticoagulant oligosaccharides for clinical use.

Materials and methods

Materials

Enoxaparin Sodium (40 mg/0.4 mL) injection was purchased from Sandoz. The AMAC and sodium cyanoborohydride were purchased from Sigma-Aldrich (St. Louis, MO, United States). Recombinant heparan lyase I, II, and III were expressed in *Escherichia coli* and purified by a Ni-agarose column. DEAE-Sepharose Fast Flow resin was purchased from GE Healthcare (Chicago, IL, United States). All reagents and chemicals were high-performance LC (HPLC) grade or LC-MS grade.

Synthesis of HS 12-mers and 18-mer

The syntheses of 12-mers were completed using the chemoenzymatic approach as described previously (Xu et al. 2017). Briefly, the synthesis was initiated from a monosaccharide pnitrophenyl glucuronide. The monosaccharide was elongated to the desired size of oligosaccharides using heparosan synthase 2. The oligosaccharides were then modified by a series of HS biosynthetic enzymes, including N-sulfotransferase, C₅epimerase, 2-O-sulfotransferase, 6-O-sulfotransferase, and 3-O-sulfotransferase 1. The 12-mer products were confirmed by ESI-MS, and its chemical purity was confirmed by highresolution anion exchange HPLC. The synthesis of 18-mer was published previously (Arnold et al. 2020). To prepare ¹³C-labeled disaccharide and trisaccharide calibrants, we synthesized ¹³C-labeled oligosaccharides. The oligosaccharides were degraded to ¹³C-labeled disaccharides using heparin lyases followed by purification using O-Sepharose as described previously (Wang et al. 2020). The ¹³C-labeled TriS (GlcNS6S-GlcA-GlcNS3S6S) was prepared freshly from heparin lyases -digested ¹³C-labeled dekaparin with a structure of GlcNS6S-[¹³C]GlcA-GlcNS3S6S-IdoA2S-GlcNS6S-IdoA2S-GlcNS6S-IdoA2S-GlcNS6S-IdoA2S-GlcNS6S-GlcA-pNP (Wang et al. 2021).

ESI-MS analysis data 12-mers and 18-mer used in the current study: The measured MW of 12-mer NAc was 2,415.7, close to the calculated MW of 2,415.0. The measured MW of 12-mer NS was 2,643.1 and matches the calculated MW of 2,643.1. The measured MW of 12-mer NS2S6S was 3,406.3, which was close to the calculated MW of 3,405.7. The measured MW of dekaparin was 3,522.8, which was close to the calculated MW of 18-mer was 4,454.2, which was close to the calculated MW of 4,455.6.

Standard curve determination

Serial dilutions of oligosaccharides were performed in 20 μ L of blank plasma and 10 μ L of blank urine collected from healthy control mice. The following concentrations and standards in Table 1 were used for the analytical studies of each oligosaccharide:

Samples and the internal standard were digested using $79.2 \,\mu\text{L}$ of enzyme cocktail containing 5 mg/mL each of heparin lyase I–III and buffer (0.1 g/L BSA, 100 mM sodium acetate, 2 mM calcium acetate, pH 7.0). The digestion was performed on the filter unit of a YM-3 kDa column (Amicon Ultra) and was incubated at $37\,^{\circ}\text{C}$ overnight. The native

Table 1.

| Oligosaccharide | Plasma (ng/µL) | Urine (ng/ μ L) | ¹³ C standard |
|-----------------|----------------|---------------------|--------------------------|
| Dekaparin | 0.15-5 | 0.31-10 | Δ IS |
| 12-mer NS2S6S | 0.62-5 | 0.15-40 | Δ IS |
| 12-mer NS | 0.16-10.5 | 5.25-168 | ΔIVS |
| 12-mer NAc | 0.15-5 | 0.15-80 | Δ IVA |
| 18-mer | 0.15-40 | 4.88–156 | ΔIIIS |

disaccharides and standards were recovered by centrifugation, and the filter unit was washed twice with $200\,\mu\text{L}$ of deionized water. The collected disaccharides were lyophilized before the AMAC derivatization. The AMAC derivatization of lyophilized disaccharides was carried out by adding $10\,\mu\text{L}$ of 0.1 M AMAC solution in DMSO/glacial acetic acid (17:3, v/v) and incubating at room temperature for 15 min. Then, $10\,\mu\text{L}$ of 1 M aqueous sodium cyanoborohydride (freshly prepared) was added to this solution. The reaction mixture was incubated at 45 °C for 2.5 h. After incubation, the reaction solution was centrifuged to obtain the supernatant that was subjected to the LC–MS/MS analysis.

LC-MS/MS analysis

The analysis of AMAC-labeled disaccharides was performed on a Vanquish Flex UHPLC System (Thermo Fisher Scientific) coupled with TSQ Fortis triple-quadrupole mass spectrometry as the detector. The C18 column (Agilent InfinityLab Poroshell 120 EC-C18 2.7 μ m, 4.6 \times 50 mm) was used to separate the AMAC-labeled disaccharides. Mobile phase A was 50 mM ammonium acetate in water. Mobile phase B was methanol. The elution gradient from 5% to 45% mobile phase B in 10 min, followed by isocratic 100% mobile phase B in 4 min, and then isocratic 5% mobile phase B in 6 min was performed at a flow rate of 0.3 mL/min. Online triplequadrupole mass spectrometry operating in the MRM mode was used as the detector. The ESI-MS analysis was operated in the negative-ion mode using the following parameters: Neg ion spray voltage at 4.0 kV, sheath gas at 45 Arb, aux gas 15 arb, ion transfer tube temp at 320 °C, and vaporizer temp at 350 °C. TraceFinder software was applied for data processing.

12-mer in vivo pharmacokinetic studies

All animal experiments were approved by the Institutional Animal Care and Use Committee of the University of North Carolina at Chapel Hill; 3–5 mice per time point were used. Control mice (0 min time point) were injected subcutaneously with equal volumes of saline and immediately sacrificed. In the 12-mer cohorts, 0.4 mg/kg of dekaparin, 12-mer NS2S6S, 12-mer NS, and 12-mer NAc were subcutaneously injected to 10-week-old male C57BL/6 J mice. Mice were sacrificed at 5, 15, 30, 45, 60, and 90 min after injection. Plasma was harvested from blood by centrifuging at 4,000 rpm for 15 min at 4 °C.

Enoxaparin and dekaparin coadministration in vivo pharmacokinetic study

In the enoxaparin/dekaparin cohort, 7.5 mg/kg enoxaparin and 0.4 mg/kg dekaparin were coinjected subcutaneously. A higher dose of enoxaparin compared to dekaparin was used because enoxaparin is detected using a unique tetrasaccharide that is in low abundance. Three mice were used per time point. Time points and sample collection is the same as above

with the addition of 120- and 240-min time points. The plasma (100 µL) was mixed with 900 µL methanol and allowed to precipitate at room temperature for 10 min. Then, the solution was centrifuged at 1,000 x g for 10 min, and the supernatant was discarded. The precipitation then was subjected to Pronase E digest (10 mg:1 g (w/w), Pronase E/protein) at 55 °C for 24 h. After digestion, the enzymatic solution was boiled at 100 °C for 10 min to denature the Pronase E and centrifuged at 14,000 rpm for 10 min to obtain the supernatant. The DEAE column (150 μ L) was used to recover the enoxaparin and dekaparin. DEAE column mobile phase A contained 20 mM Tris, pH 7.5, and 50 mM NaCl, and mobile phase B contained 20 mM Tris, pH 7.5, and 1 M NaCl. After loading the sample into DEAE column, the column was washed with 1.5 mL mobile phase A, followed by 1.5 mL mobile phase B to elute the enoxaparin fraction. The eluted enoxaparin and dekaparin were desalted using an YM-2KDa (Sartorius) spin device and the device washed 3 times with deionized water. The spin device was reversed to recover the retentate from the membrane and washed 3 times with deionized water. The combined solution was dried before the digestion with heparin lyases. The 100 μ L of enzymatic buffer (100 mM sodium acetate/2 mM calcium acetate buffer (pH 7.0) containing 0.1 g/L BSA) and 6 μ L of enzyme cocktails containing 5 mg/mL each of heparin lyase I, II, and III was added to digest enoxaparin at 37 °C overnight. The digestion solution was boiled at 100 °C for 10 min and centrifuged at 14,000 rpm for 10 min to recover the disaccharides. The supernatant was recovered and freezedried before the AMAC labeling step.

18-mer and APAP model in vivo pharmacokinetic study

In the 18-mer APAP cohort, mice were fasted overnight (12-15 h) to deplete glutathione stores before APAP (Sigma) administration; 3-5 mice were used per time point. Fresh APAP was dissolved in warm (~50 °C) sterile saline, cooled to 37°C, and injected intraperitoneally at 400 mg/kg to induce APAP overdose. The healthy control mice were injected with saline intraperitoneally. Three hours post-APAP or saline injection, 0.4 mg/kg 18-mer was subcutaneously administered. Healthy mice were sacrificed at the time points described above. APAP-overdose mice were sacrificed at 5, 15, 30, 45, 60, 90, 120, and 150 min after 18-mer injection. In the modified dose cohort, mice were fasted overnight and intraperitoneally injected with 400 mg/kg APAP. Three hours post-APAP overdose, 0.4 mg/kg or 2.4 mg/kg 18-mer was subcutaneously injected. Fifteen hours post-APAP overdose, 0.4 mg.kg 18-mer was administered to the 2injection cohort. All mice were sacrificed at 24 h post-APAP overdose.

Biomarker assay

Plasma was collected for ALT determination using the ALT Infinity reagent (Thermo Fisher) following the manufacturer's instructions. Plasma HMGB1 concentrations were determined using HMGB1 ELISA Kit (Tecan US) according to the manufacturer's instructions. Plasma creatinine was determined using a kit (Crystal Chem) according to the manufacturer's instructions.

LC-MS/MS analysis of plasma and urine samples

The 20 μ L of plasma or 10 μ L of urine were used for analysis; 50 ng of the appropriate 13 C-labeled internal standard were added to each sample. Samples were prepared and analyzed as described above in standard curve determination and LC–MS/MS analysis.

Chromogenic FXa assay

Human FXa (Enzyme Research Laboratories) was diluted to 50 U/mL with PBS. The chromogenic substrate S-2765 (Diapharma) was diluted to 1 mg/mL in water. Dekaparin was serially diluted in control mouse plasma (0.078–10 ng/ μ L) to obtain a standard curve. The 10 μ L of dekaparin plasma sample and standards were incubated with 60 μ L of 34 μ L/mL antithrombin (Cutter Biologics) in 1 mg/mL BSA for 2 min at room temperature. Next, 100 μ L of FXa was added and incubated for 4 min at room temperature. The 30 μ L of S-2765 substrate was added and the absorbance of the reaction mixture was measured at 405 nm continuously for 2 min. Blank plasma serves as a control sample. The maximum slope for each sample was converted to percent FXa activity by dividing by the maximum slope for the control sample.

Software

NCA was performed to determine pharmacokinetic parameters using Phoenix 64 Win Nonlin software 8.3.5.340. NCA was calculated using linear trapezoidal linear interpolation with a plasma model type and extravascular dose option. AUC was calculated from the time of dosing to the time of the last observation (AUC_{all}). Graphs were created using GraphPad Prism Version 8. Statistics were performed using GraphPad Prism. Illustrations were created using BioRender.com.

Results

Preparation of HS oligosaccharides and ¹³C-labeled oligosaccharide calibrants

Pharmaceutical heparin and HS isolated from biological sources are mixtures of polysaccharides with different lengths of sugar chains and sulfation patterns. To investigate the contribution of sulfation to the pharmacokinetic properties, we employed 4 different structurally homogeneous 12-mers (Table 2). The 4 12-mers included nonsulfated 12-mer (12mer NAc) to fully sulfated 12-mer (dekaparin). Several ¹³Clabeled calibrants were also synthesized in the study. These ¹³C-labeled calibrants include 4 ¹³C-labeled disaccharides, a C¹³-labeled sulfated trisaccharide (TriS), and a ¹³C-labeled sulfated tetrasacchatide (ΔTetraS) (Table 2). The structures of the calibrants match the products from the 12-mers and enoxaparin after the digestion with heparin lyases, as shown in Table 2. For example, 13 C-labeled Δ IVA was suited for the analysis of 12-mer NAc, whereas 13 C-labeled Δ IS was suited for the analysis of dekaparin. The unlabeled 12-mers and ¹³C-labeled calibrants were synthesized using the chemoenzymatic approach and their structures were confirmed by electrospray ionization mass spectrometry (ESI-MS) as previously published (Xu et al. 2014; Wang et al. 2020).

Table 2. List of ¹³C-labeled calibrants used for the bioanalytical analysis of 12-mers, enoxaparin, and 18-mer.

| Name | Abbreviated full sequence | Products after heparin lyase digestion | | ¹³ C-labeled calibrants used | |
|---------------|--|---|------------------------------|--|---|
| | | Abbreviated | Shorthand used | Abbreviated | Shorthand used in text |
| 12-mer NAc | GlcNAc-GlcA-GlcNAc- GlcA-GlcNAc-GlcA- GlcNAc-GlcA-GlcNAc- GlcA-GlcNAc-GlcA-pNP | ΔUA-GlcNAc | ΔIVA | [U- ¹³ C]ΔUA- GlcNAc ^a | ¹³ C-labeled∆IVA |
| 12-mer NS | GleNS-GleA-GleNS- GleA-GleNS-GleA- GleNS-GleA-GleNS- GleA-GleNS-GleA-pNP | ΔUA-GlcNS | ΔIVS | [U- ¹³ C]ΔUA-GlcNS | ¹³ C-labeled ΔIVS |
| 12-mer NS2S6S | GlcNS6S-GlcA-GlcNS6S- IdoA2S-GlcNS6S-IdoA2S- GlcNS6S-IdoA2S- GlcNS6S-IdoA2S- GlcNS6S-GlcA-pNP | ΔUA-GlcNS6S and ΔUA2S-GlcNS6S | Δ IIS and Δ IS | [U- ¹³ C]ΔUA2S- GlcNS6S ^b | ¹³ C-labeled ΔIS |
| dekaparin | GlcNS6S-GlcA- GlcNS3S6S-IdoA2S- GlcNS6S-IdoA2S- GlcNS6S-IdoA2S- GlcNS6S-IdoA2S- GlcNS6S-GlcA-pNP | AUA2S-GlcNS6S and GlcNS6S-GlcA- GlcNS3S6S | ΔIS and TriS | [U- ¹³ C]ΔUA2S- GlcNS6S and GlcNS6S- [U- ¹³ C]GlcA- GlcNS3S6S ^c | $^{13}\text{C-labeled}$ ΔIS and $^{13}\text{C-labeled}$ TriS |
| enoxaparin | Mixture of oligosaccharides, no defined sequence | Eight disaccharides and ΔUA-GlcNAc6S- GlcA-GlcNS3S6S | ΔTetraS | ΔUA-GlcNAc6S- [U- ¹³ C]GlcA- GlcNS3S6S | ¹³ C-labeled ΔTetraS |
| 18-mer | GlcNS-GlcA-GlcNS- IdoA2S-GlcNS-IdoA2S- GlcNS-IdoA2S-GlcNS- IdoA2S-GlcNS-IdoA2S- GlcNS-IdoA2S-GlcNS- IdoA2S-GlcNS-GlcA-pNP | ΔUA2S-GlcNS | ΔIIIS | [U- ¹³ C]∆UA2S- GlcNS | ¹³ C-labeled ΔIIIS |

 a [U- 13 C] Δ UA represents universally 13 C-labeled $\Delta_{4,5}$ -unsaturated uronic acid. b [U- 13 C] Δ UA2S represents universally 13 C-labeled $\Delta_{4,5}$ -unsaturated uronic acid 2-O-sulfate. c ¹³C-labeled TriS is unstable due to the presence of a GlcNS3S6S residue at the reducing end (Huang et al. 2015; Dhurandhare et al. 2020). The 13 C-labeled TriS was freshly generated from 13 C-labeled dekaparin after the digestion with heparin lyases at the time that the analysis was performed. d13 C-labeled Δ TetraS is unstable due to the presence of a GlcNS3S6S at the reducing end. The 13 C-labeled Δ TetraS was freshly generated from a 13 C-labeled 8-mer (GlcNAc-GlcA-GlcNAc6S-[U- 13 C]GlcA-GlcNS3S6S-IdoA2S-GlcNS6S-GlcA-pNP) after the digestion with heparin lyases at the time that the analysis was performed.

Pharmacokinetics of 12-mers in plasma and urine

We chose dekaparin to validate the LC-MS/MS method in the initial study. The LC-MS/MS method involves 3 steps, including heparin lyases degradation, chemical derivatization, and LC-MS/MS analysis, as illustrated in Fig. 1A. Dekaparin (\sim 10 μ g, or 0.4 mg/kg) was injected subcutaneously to mice and blood samples were collected 5-90 min later. The plasma samples were subjected to the digestion with heparin lyases to yield Δ IS (Δ UA2S-GlcNS6S) disaccharide and TriS trisaccharide (GlcNS6S-GlcA-GlcNS3S6S; Fig. 1A). Here, Δ IS was used for determining the concentration of dekaparin. The $^{13}\text{C-labeled}$ ΔIS calibrant (50 ng) was added to the samples prior to 3-aminoacridin-9-(10H)-one (AMAC) derivation (step 2). Coupling an AMAC hydrophobic tag to disaccharides increases the binding affinity to a C₁₈-column and improves the resolution of different disaccharides by the C₁₈-column, facilitating the analysis (Li et al. 2015). The samples were then analyzed by the LC-MS/MS analysis, where multiple reaction monitoring (MRM) analysis was performed to gain sensitive measurements. A response signal from the native Δ IS and ¹³C-labeled Δ IS was obtained with molecular mass differed by 6 Da (step 3, Fig. 1A). Determination of the ratio of the areas of native ΔIS peak and ¹³C-labeled

 Δ IS peak allowed us to determine the plasma concentrations of dekaparin (Supplementary Fig. S1). A standard curve plotting the concentrations of dekaparin against the ratio of native and ¹³C-labeled Δ IS was generated, showing a linear response that was suited for the quantitative analysis (Supplementary Fig. S2).

The plasma concentration versus time profile of dekaparin is shown in Fig. 1B. Dekaparin concentration peaked between 30 and 45 min after the injection and decreased after 60 min (Fig. 1B).

Dekaparin has anti-FXa activity, which can be used to determine the concentration in plasma to validate the measurement from the LC-MS/MS analysis (Xu et al. 2017). This anti-FXa method is designed to determine the degree of inhibition of FXa and is widely used to measure the concentrations of anticoagulant HS and LMWHs (Xu et al. 2017). The elimination profile of dekaparin as measured by anti-FXa method is shown in Fig. 1B. When visualized using a Bland-Altman plot to estimate the agreement between the 2 methods, all data fall within the limits of agreement calculated by the 95% confidence interval (CI; Fig. 1C; Giavarina 2015). In addition, LC-MS/MS analysis offers an excellent linear response across a wide range of concentrations, and the values from the LC-MS/MS determinations were more closely clustered

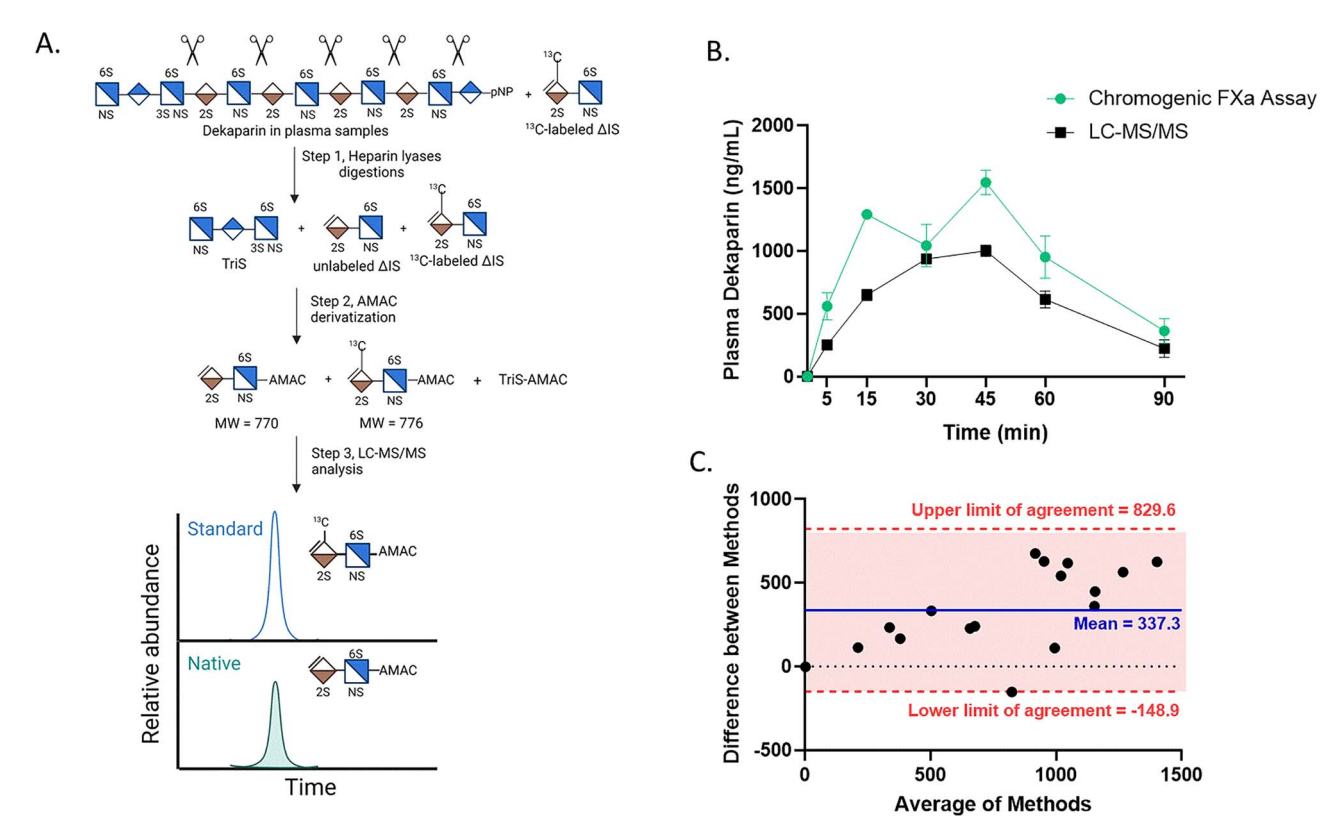


Fig. 1. Analysis of depakarin using the LC-MS/MS analysis. A) Workflow depiction for the analysis of dekaparin using the LC-MS/MS analysis. Three steps are involved in the procedure as described in the text. Representative MRM ion chromatograms are illustrated in step 3. B) Elimination curve of dekaparin measured by the LC-MS/MS method and the anti-FXa assay. Data represent mean \pm SEM (n=3 per time point). C) Bland-Altman plot showing the difference between paired measurements of the LC-MS/MS and anti-FXa assay versus the average of the paired differences between methods. The mean of the differences is represented by a solid line. The upper and lower limits of agreement are represented by bold dashed lines. The shaded red area between the limits of agreement is the 95% CI.

than those values determined by the anti-FXa assay method. Taken together, our results confirmed that the LC-MS/MS method is an appropriate method to perform the quantitative analysis of HS oligosaccharides for the pharmacokinetic analysis.

Next, pharmacokinetic studies of 4 12-mers were performed after subcutaneous injection of 0.4 mg/kg in mice. Plasma samples were analyzed by the LC-MS/MS method (Fig. 2). Among the 4 12-mers, only dekaparin inhibits the activity of FXa because it contains the specific pentasaccharide structure required for antithrombin binding (Xu et al. 2017). The other 12-mers have less sulfation than dekaparin and do not inhibit the activity of FXa (Fig. 2A). 12-mer NS2S6S, 12-mer NS, and 12-mer NAc are designated as nonanticoagulant 12-mers. Since the traditional method for detecting heparin drug concentration relies on measuring FXa inhibition, the concentration of nonanticoagulant 12-mers can only be determined by LC-MS/MS. Each 12-mer was subjected to the workflow shown in Fig. 1A with appropriately selected ¹³C-labeled disaccharide calibrants (Table 2). Standard curves for each 12-mer were prepared, as shown in Supplementary Fig. S2, showing excellent linear responses between the concentration of 12-mer and the ratio area of the native and ¹³C-labeled disaccharide peaks in both plasma and urine. The elimination profiles from plasma for 12mers are shown in Fig. 2B. We obtained the pharmacokinetic parameters for each 12-mer by noncompartmental analysis (NCA) using Phoenix WinNonLin software (Fig. 2C).

Among the 3 nonanticoagulant 12-mers, 12-mer NS2S6S had the smallest AUC and C_{max} (7.1 vs. 12.8–12.9 μ g/mL•min and 0.18 vs. 0.27–0.38 μ g/mL, respectively). Compared to 12-mer NAc and 12-mer NS, the average concentration across all time points was lower in 12-mer NS2S6S treated mice (Fig. 2B). However, dekaparin had a plasma AUC value of 56.6 μg/mL•min, which is 4.4-fold to 8.0-fold higher than that of other 12-mers. A higher AUC value suggests that dekaparin has higher overall systemic exposure after administration. The maximum concentration (C_{max}) values also reflect this trend with the nonanticoagulant 12-mers having a C_{max} that is 2.6-5.7 times lower than that of dekaparin (Fig. 2B and C). Accordingly, the average concentration across all time points was significantly higher in the dekaparin treated mice reflected by P-values < 0.0001 compared to each nonanticoagulant 12-mer (Fig. 2B). The nonanticoagulant 12-mers have similar clearance (Cl) values ranging from 29 to 54 mL/min, while the Cl value for anticoagulant dekaparin was 6.3 mL/min (Fig. 2B). Overall, there are small PK differences among the nonanticoagulant oligosaccharides and dramatic PK differences between nonanticoagulant and anticoagulant 12-mers.

Urine analysis revealed that the relative concentration of dekaparin in the urine is much lower than the nonanticoagulant 12-mers (Fig. 2D). For example, the concentration of dekaparin in urine was about the same as in the plasma at 45 min; however, the concentration of 12-mer NS2S6S was 28.8-fold higher in urine than in plasma at 45 min.

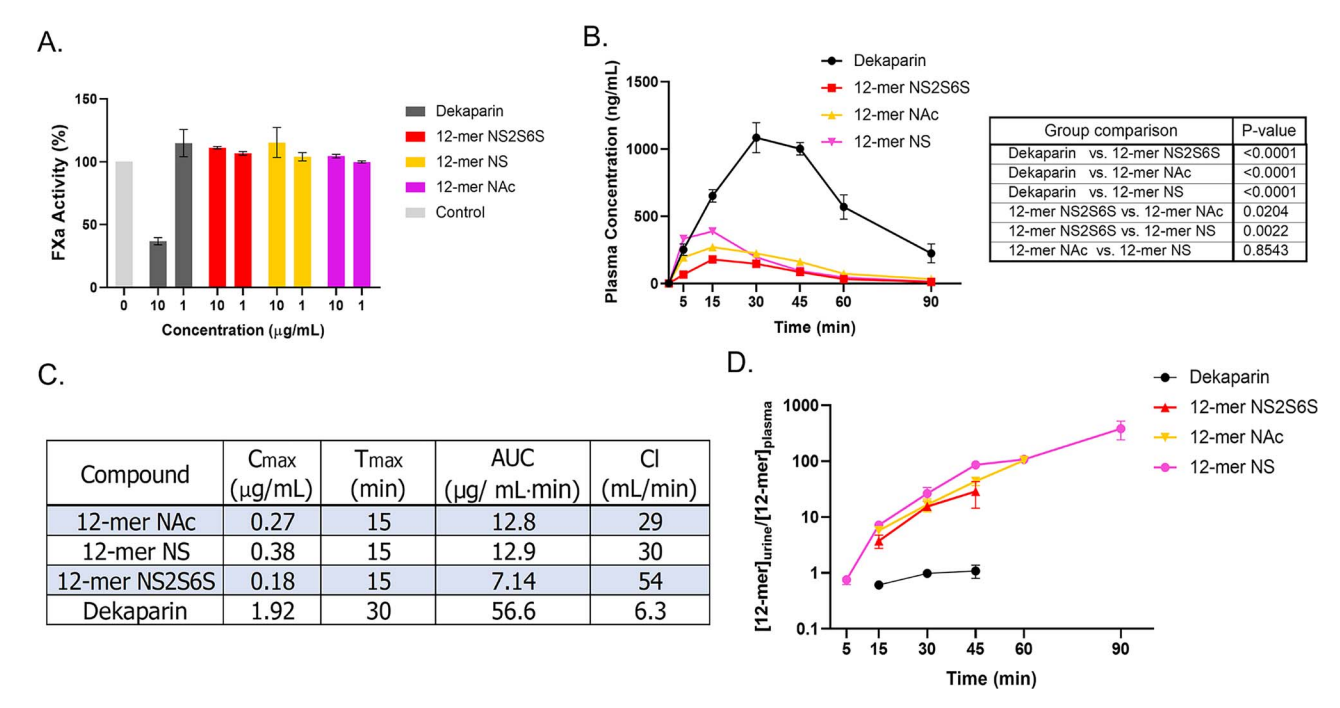


Fig. 2. Pharmacokinetic parameters of 12-mer panel. A) In vitro FXa activity of 12-mers determined at 10 and 1 μ g/mL. B) Plasma elimination of 12-mers after subcutaneous injection. C) C_{max} , time of maximum concentration (T_{max}), AUC, and Cl values for 12-mers. D) Ratio of urine-to-plasma concentration over time. Data represent mean \pm SEM (n = 3–5). P-values determined by 2-way ANOVA with Dunnett's multiple comparisons posttest.

Our data suggest that 12-mers are rapidly renally eliminated. Interestingly, the overall level of sulfation does not alter the renal clearance. Among the 4 12-mers tested, only dekaparin binds to antithrombin, a key protein that inhibits the activities of thrombin and FXa. One possible explanation for dekaparin's lower clearance rate is that it forms a complex with antithrombin that is abundant in plasma. It has previously been shown that a subpopulation of daltaparin polysaccharides, an LMWH, with high affinity to antithrombin, had a lower clearance compared to low-affinity polysaccharide population (Stehle et al. 1997). Similar to our findings with the nonanticoagulant 12-mers, low-affinity polysaccharides were rapidly renally excreted.

Dekaparin and anticoagulant enoxaparin have similar plasma disposition in mice

As a candidate to replace animal sourced LMWH, dekaparin is undergoing preclinical studies (Xu et al. 2017). We intended to determine whether dekaparin and LMWH have similar pharmacokinetic profiles. Here, we used the LC-MS/MS method to compare the elimination profiles of dekaparin and enoxaparin, an LMWH, in a mouse model. To accurately compare the elimination rates of dekaparin and enoxaparin, compounds were coadministered in a single injection and the concentrations of dekaparin and enoxaparin were determined. Following specific saccharide markers, the LC-MS/MS method enabled us to separately measure dekaparin and enoxaparin from the same plasma sample. Enoxaparin is a mixture of oligosaccharides with different sizes and sulfated saccharide sequences. The mixture contains both anticoagulant and nonanticoagulant subpopulations; however, only the analysis of anticoagulant subpopulation of enoxaparin is relevant to the current study. A unique tetrasaccharide (ΔUA-GlcNAc6S-GlcA-GlcNS3S6S, or ΔTetraS in

Table 2) was liberated from enoxaparin after the digestion with heparin lyases (Fig. 3A). This tetrasaccharide was reportedly associated with the anticoagulant subpopulation from enoxaparin and thereby used as a marker for the anticoagulant enoxaparin (Sundaram et al. 2003; Chen et al. 2017; Wang et al. 2022). Distinct from enoxaparin, dekaparin yielded 1 trisaccharide (GlcNS6S-GlcA-GlcNS3S6S, or TriS, as shown in Table 2) after the digestion with heparin lyases. This trisaccharide is absent in heparin lyases-degraded enoxaparin (Fig. 3A). Use of Δ TetraS and TriS markers allowed us to measure the concentrations of dekaparin and enoxaparin in a single batch of LC-MS/MS analysis.

The plasma concentration profiles of enoxaparin and dekaparin were similar, as shown in Fig. 3B, confirming that they have similar PK dispositions after injection. The AUCs for enoxaparin and dekaparin are 147.1 and 215.6 μ g/mL•min, respectively. It should be noted that the selection of Δ IS disaccharide marker did not separate dekaparin and enoxaparin because both dekaparin and enoxaparin yield Δ IS after the digestion with heparin lyases. It has also been reported that the anticoagulant subpopulation in LMWH contains different sizes (Bisio et al. 2009). Our findings should not be construed that different anticoagulant sugar chains are cleared at the same rate.

The pharmacokinetic clearance of nonanticoagulant 18-mer is reduced in mice after acute liver injury induced by acetaminophen overdose

We next investigated the impact of disease state on synthetic heparan sulfate pharmacokinetics. We evaluated the pharmacokinetic disposition of 18-mer in 10-week-old C57BL6/J male mice after acetaminophen (APAP) induced acute liver injury and compared these results to healthy mice. The 18-mer

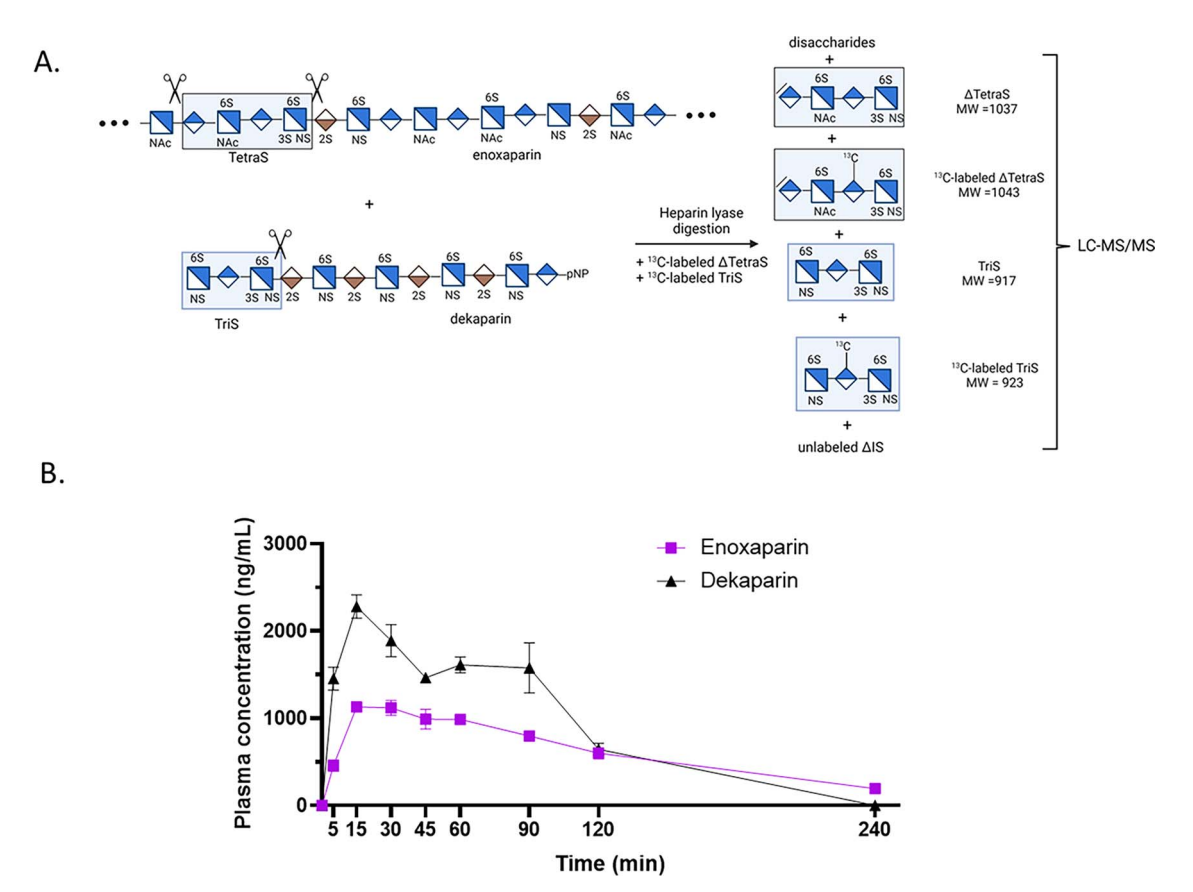


Fig. 3. Comparison of the clearance between dekaparin and enoxaparin. A) Enzymatic digestion reaction of dekaparin and enoxaparin using the mixture of heparin lyases. ^{13}C Δ TetraS is added for enoxaparin measurement and ^{13}C TriS is added for dekaparin measurement. B) Elimination profile of dekaparin and enoxaparin. Data represent mean \pm SEM (n = 3).

was previously shown to display protection against liver damage by interacting with high mobility group box-1 (HMGB1), a proinflammatory protein released from hepatocytes upon the injury (Arnold et al. 2020). Our hypothesis is that the clearance of 18-mer is slowed after the acute liver injury, resulting in longer drug exposure and sustained protection in vivo. To this end, we evaluated the pharmacokinetic disposition of 18-mer in both healthy mice and APAPoverdose mice using the LC-MS/MS method (Fig. 4). The ¹³C-labeled ΔIIIS calibrant was used in the analysis of 18mer (Table 2). Standard curves for 18-mer in plasma and urine were prepared, as shown in Supplementary Fig. S3, showing excellent linear responses between the concentration of 18-mer and the ratio area of the native and ¹³C-labeled disaccharide peaks. In healthy mice, the plasma concentration of 18-mer peaked around 15 min after subcutaneous injection and was completely cleared by 90 min (Fig. 4B). This result indicated that 18-mer is cleared fast like the nonanticoagulant 12-mers. However, in APAP-overdose mice, the elimination profile of 18-mer was substantially slowed (Fig. 4B). The plasma concentration of 18-mer in APAP-overdose mice was significantly higher between 60 and 90 min compared to healthy mice (Fig. 4B) and remained detectable at 150 min after injection. In line with the decreased rate of clearance, the AUC value from APAP-overdose mice was also 2.2-fold greater than that in healthy mice (Fig. 4A). In the urine, healthy mice have higher urine-to-plasma concentration ratios at the time points between 45 and 60 min (Fig. 4C). Taken together, our results suggest that the clearance of 18-mer is slowed after APAP overdose.

We investigated whether there was a change of plasma proteins after APAP overdose. Specifically, we focused on 18mer-binding protein, i.e. HMGB1. In this animal model, APAP overdose causes hepatocyte necrosis, resulting in the release of a nucleic protein, known as HMGB1, with proinflammatory activity. HMGB1 recruits neutrophils, which further damages hepatocytes and contributes to dysregulated sterile inflammatory response after the initial injury (Huebener et al. 2015). We measured the plasma concentrations of alanine aminotransferase (ALT), creatinine, and HMGB1 at 3 h after APAP overdose (Fig. 5). The plasma concentrations of ALT and creatinine are common markers to assess the damage to liver and kidney, respectively. Elevated ALT and unchanged creatinine level suggested that APAP overdose caused liver damage while the function of kidney was unaffected (Fig. 5A and B). During the pharmacokinetic analysis, average plasma ALT was 351 U/L, suggesting that minimal liver damage has occurred after 3 h. This result is expected because the extensive liver damage is typically observed at 24 h after APAP overdose, resulting in ALT levels as high as 4,000-5,000 U/L (Arnold et al. 2020). Despite limited damage at 3 h in this experiment, an elevated concentration of HMGB1 was clearly obvious (Fig. 5C). HMGB1 reportedly binds to 18-mer with an affinity of 186 nM (Arnold et al. 2020). A high plasma concentration of HMGB1 potentially slows down the clearance of 18-mer by forming a complex between HMGB1 and 18-mer.

We redesigned the 18-mer treatment regimen by reducing the number of injections to take advantage of the longer exposure and slower clearance of 18-mer in APAP-overdose

| А | | |
|---|--|--|
| | | |
| | | |

| | Cmax | Tmax | AUC | Cl |
|----------------|--------------|-------|-------------|----------|
| Compound | $(\mu g/mL)$ | (min) | (µg/mL·min) | (mL/min) |
| 18-mer 2S | 0.20 | 15 | 9.69 | 39 |
| APAP 18-mer 2S | 0.23 | 15 | 21.6 | 14 |

B. C.

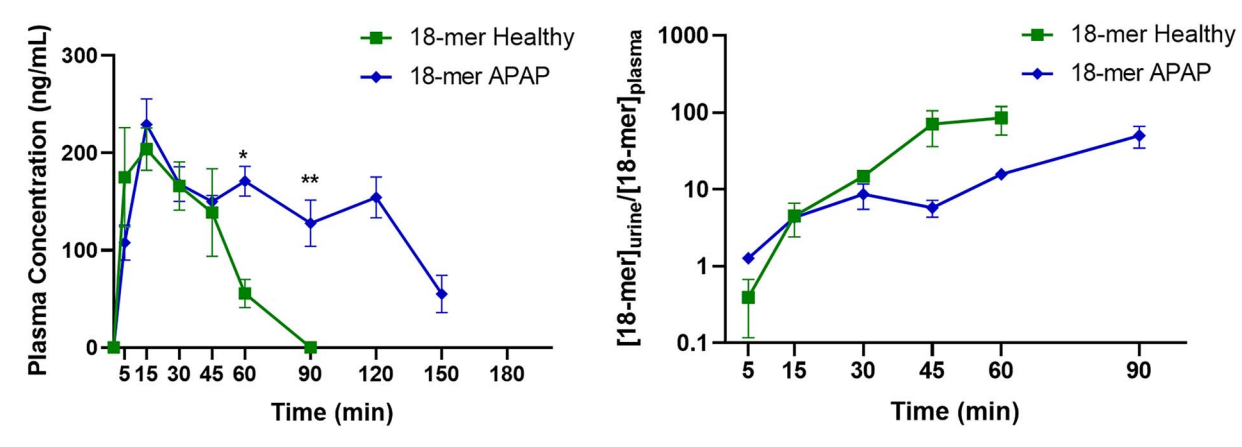


Fig. 4. Pharmacokinetics of 18-mer in healthy and APAP injured mice. A) C_{max} , T_{max} , AUC, and CI values for 18-mer in healthy and APAP-overdose mice; 0.4 mg/kg of 18-mer was subcutaneously administered 3 h after APAP overdose. B) Plasma concentration over time in healthy and APAP-overdose mice. C) Ratio of urine-to-plasma concentration over time in healthy and APAP-overdose mice. Data represent mean \pm SEM (n=3–5). *, P<0.05; **, P<0.01 determined by 2-way ANOVA with Sidak's multiple comparisons posttest. The standard curves for the measurement of 18-mer in plasma and urine are shown in Supplementary Fig. S2.

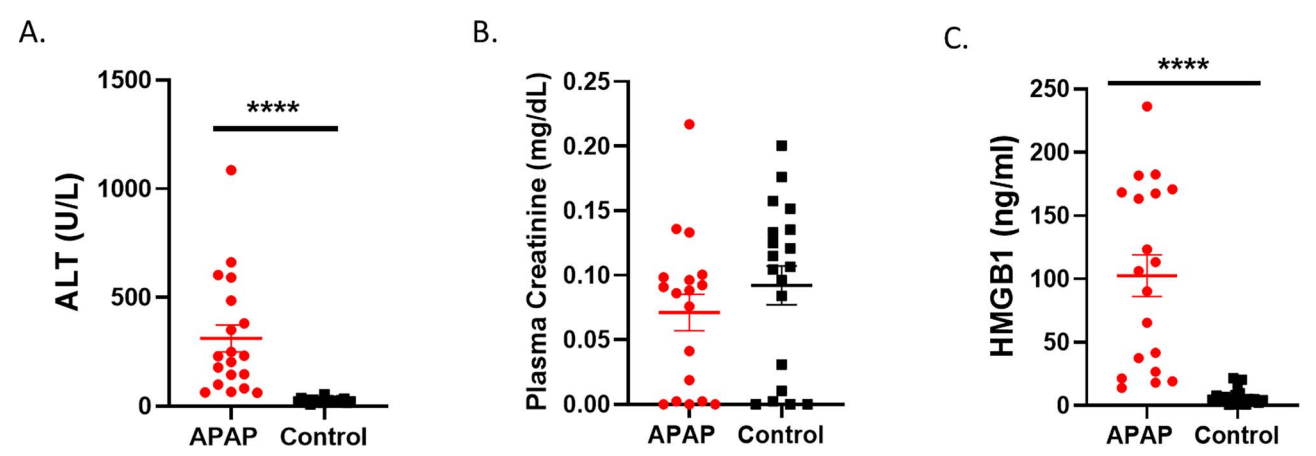


Fig. 5. Biochemical markers of injury. A) Plasma ALT, a liver injury biomarker, is significantly higher in APAP-overdose mice compared to control. B) Plasma creatinine, a kidney function marker, is the same between groups. C) Plasma HMGB1 concentration in APAP overdose is significantly higher compared to control mice. Data represent mean \pm SEM. *****, P < 0.0001 determined by t-test.

mice. In our previously reported dosing strategy, we administered 0.4 mg/kg 18-mer at 3 and 15 h post-APAP overdose (Arnold et al. 2020). Here, we elevated the dosing strategy to 2.4 mg/kg 18-mer in a single injection at 3 h post-APAP. Interestingly, the alternative dosing regimen displayed protection as measured by the plasma concentration of ALT in a side-by-side comparison (Fig. 6A). In fact, a single, high dose of 18-mer given at 3 h post-APAP even decreased the ALT compared to the original two dose regimen (Fig. 6B). Currently, infusion of *N*-acetylcysteine is the standard treatment for APAP-overdose patients in hospitals. However, the treatment is only effective if APAP overdose occurred within 8 h (Bailey et al. 2016). Previously, we demonstrated that 18-mer is effective for delayed treatment in mice, which potentially widens the therapeutic window for APAP-overdose patients

(Arnold et al. 2020). Simplifying the treatment regimen to a single injection will add further advantage of using 18-mer to treat APAP-overdose patients.

Discussion

Here, we report the pharmacokinetic analysis of structurally homogeneous HS oligosaccharides in mice using an LC–MS/MS method. Compared to previous detection methods, this is the first method to detect the structure of exogenous nonlabeled oligosaccharides quantitatively. The LC–MS/MS method relies on the degradation of oligosaccharides into disaccharides and the use of isotopically labeled disaccharide internal standards for quantitation. The method was developed using dekaparin, an anticoagulant 12-mer. We compared

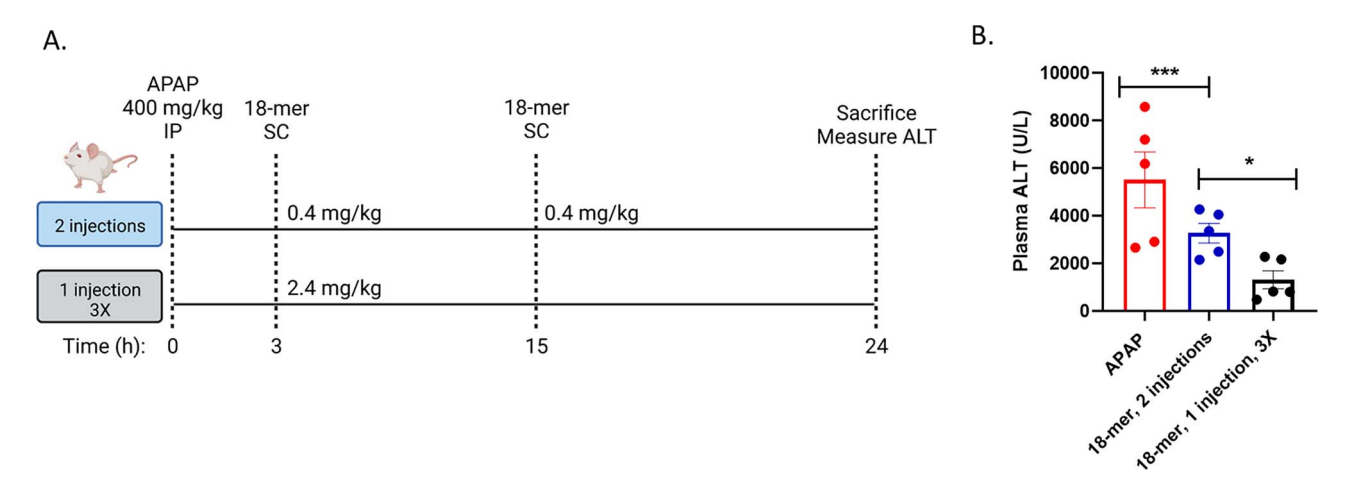


Fig. 6. Modified dose regimen after APAP overdose. A) Illustration of experimental design. The "2 injection" scheme depicted on the top represents the original dose regimen. The "1 injection 3X" scheme depicted on the bottom represents the optimized dose regimen. B) ALT from a single injection at 3X 18-mer concentration is significantly lower than the 2-injection regimen. Data represent mean \pm SEM. *, P < 0.05; ***, P < 0.001 determined by 1-way ANOVA with Tukey's multiple comparisons posttest.

the plasma concentration determined by LC–MS/MS to the result from the anti-FXa chromogenic assay, which is clinically used to measure anticoagulant heparin and LMWH. This activity assay is used to determine the concentration of heparin and LMWH and relies on indirectly measuring the fraction of anticoagulant oligosaccharides in the mixture. The results from both the LC–MS/MS and anti-FXa methods agree with each other, validating the LC–MS/MS method.

The LC-MS/MS method was also applied to analyze the pharmacokinetic properties of 3 12-mers with varying sulfation patterns that lack anticoagulant activity. Unexpectedly, we discovered that all 3 nonanticoagulant 12-mers display similar exposure and elimination in mice despite the different sulfation levels. Anticoagulant dekaparin displayed significantly slower clearance and longer exposure in plasma than the other 3 12-mers. The critical differentiating structural factor of dekaparin is the 3-O-sulfated glucosamine residue that allows for antithrombin binding. Our findings support the conclusion that the binding event of dekaparin to antithrombin may affect dekaparin's pharmacokinetics (Damus et al. 1973). The influence of protein binding on heparin and LMWH pharmacokinetics has been proposed in the past (Palm and Mattsson 1987; Stehle et al. 1997). These studies separated radiolabeled LMWH into fractions based on high and low affinities for antithrombin to assess pharmacokinetics based on the radioactive measurement. LMWH fractions with low affinity to antithrombin have a lower plasma AUC and are excreted faster than high affinity fractions (Palm and Mattsson 1987; Stehle et al. 1997). A recent paper confirmed that the anticoagulant subpopulation of enoxaparin is cleared slower than the nonanticoagulant subpopulations in mice (Wang et al. 2022), which is consistent with our findings presented in the current studies using structurally homogeneous 12-mers.

Dekaparin is reportedly cleared through the binding to both stabilin-1 and stabilin-2 receptors found in liver sinusoidal endothelial cells (Harris and Cabral 2019). Both receptors participate in the clearance of 3-O-sulfated HS oligosaccharides (Pempe et al. 2012). The [35 S]-radioactively labeled n12-mer, a nonanticoagulant 12-mer that has the same structure

of NS2S6S 12-mer used in the current study, displayed significantly higher concentration in urine than in liver, suggesting that n12-mer is cleared from kidney. By contrast, radioactively labeled dekaparin showed lower concentration in urine than in liver, suggesting that dekaparin is partially eliminated by liver (Miller et al. 2018). Furthermore, the clearance of dekaparin was impaired in a severe kidney injury mouse model, confirming that the kidney is also involved in the clearance of dekaparin (Xu et al. 2017).

The findings from the pharmacokinetic analysis of HS 18-mer offers new insights on the factors that influence the clearance of HS oligosaccharides under different physiological or pathophysiological conditions. As an emerging new class of antiinflammatory agents, understanding the dynamics of HS pharmacokinetics is essential for the advancement of HS-based therapeutics. We recently reported on an antiinflammatory 18-mer that protects from liver damage in a model of APAP-induced acute liver failure (Arnold et al. 2020). Pharmacokinetic and pharmacodynamic analyses are critical for further preclinical development of 18-mer. In healthy mice, the plasma concentration of HMGB1 is low and the 18-mer is cleared rapidly from the circulation. In the APAP-overdose model, 18-mer binds to circulating proinflammatory HMGB1 and has a slower clearance compared to healthy mice. We hypothesize that the difference in pharmacokinetics in the APAP model translates to a beneficial hepatoprotection effect. In theory, as inflammation and HMGB1 levels are subsiding during the recovery phase, 18-mer will return to fast clearance. This property may minimize potential side effects, making the 18-mer an effective and safe candidate as an antiinflammatory agent.

Heparin and LMWH are widely used anticoagulant drugs to treat thrombotic disorders. The antiinflammatory effects of heparin and LMWH have been increasingly noticed (Liu et al. 2020). Notably, heparin was recently recommended for the treatment of critically and noncritically ill COVID-19 patients (Attacc et al. 2021; REMAP-CAP et al. 2021). A clear understanding to the pharmacokinetics of nonanticoagulant subpopulation in heparin and LWMH will help improve the treatment of heparin and LMWH for COVID-19 patients.

Typically, the anti-FXa assay is unsuited to analyze nonantico-agulant heparin and LMWH. The LC-MS/MS method offers the sensitivity and throughput for carrying out the studies.

Acknowledgements

Authors are thankful for the access to Phoenix Win Nonlin software, which was generously provided to the UNC Eshelman School of Pharmacy by Certara, Inc, through their Center of Excellence program.

Supplementary material

Supplementary material is available at GLYCOB Journal online.

Funding

This work is supported in part by National Institutes of Health (grant numbers HL094463, HL144970, GM142304, and GM144019) and Glycan Innovation grants from Eshelman Innovation Institute. This work is also supported by GlycoMIP, a National Science Foundation Materials Innovation Platform funded through Cooperative Agreement DMR-1933525.

Conflict of interest statement: JL and YX are founders of Glycan Therapeutics. JL is the chief scientific officer for Glycan Therapeutics. KA holds a part time appointment as a Scientist at Glycan Therapeutics. Other authors declare no competing interest.

Data availability

LC-MS/MS data and structural characterization of oligosaccharides and 13C standards are available upon request to the authors.

Abbreviations

ALT, alanine aminotransferase; AMAC, 3-aminoacridin-9-(10H)-one; APAP, acetaminophen; AUC, area under the curve; Cl, clearance; $C_{\rm max}$, maximum concentration; ESI-MS, electrospray ionization mass spectrometry; FXa, factor Xa; HMGB1, high mobility group box-1; HS, heparan sulfate; LC–MS/MS, liquid chromatography coupled with tandem mass spectrometry; LMWH, low molecular weight heparin; MRM, multiple reaction monitoring; NCA, noncompartmental analysis; Δ TetraS, 13 C-labeled sulfated tetrasaccharide; $T_{\rm max}$, time of maximum concentration; TriS, C^{13} -labeled sulfated trisaccharide; UFH, unfractionated heparin.

References

- Arnold KM, Xu Y, Sparkenbaugh EM, Li M, Han X, Zhang X, Xia K, Peiegore M, Li M, Zhang F, et al. Design of anti-inflammatory heparan sulfate to protect against acetaminophen-induced accute liver failure. *Sci Transl Med*. 2020:12:eaav8075.
- Attacc T, Activ-4a, Remap-cap I. Therpaeutic anticoagulation with heparin in noncrtically ill patients with Covid-19. N Engl J Med. 2021:385:790–802.
- Baglin T, Barrowcliffe TW, Cohen A, Greaves M, Haematology, B.C.f.S.i. Guidelines on the use and monitoring of heparin. Br J Haematol. 2006:133:19–34.
- Bailey GP, Najafi J, Elamin ME, Waring WS, Thomas SH, Archer JR, Wood DM, Dargan PI. Delays during the administration of acetylcysteine for the treatment of paraacetamol overdose. Br J Clin Pharmacol. 2016:62:1358–1363.
- Bisio A, Vecchietti D, Citterio L, Guerrini M, Raman R, Bertini S, Eisele G, Naggi A, Sasisekharan R, Torri G. Structural features of low-molecular-weight heparins affecting their affinity to antithrombin. Throm Haemost. 2009:102:865–873.

Chen Y, Lin L, Agyekum I, Zhang X, St. Ange K, Yu Y, Zhang F, Liu J, Amster IJ, Linhardt RJ. Structural analysis of heparin-derived 3-O-sulfated tetrasaccharides: antithrombin binding site variants. *J Pharm Sci.* 2017:106:973–981.

- Clausen TM, Sandoval DR, Spliid CB, Pihl J, Perrett HR, Painter CD, Narayanan A, Majowicz SA, Kwong EM, McVicar RN, et al. SARS-CoV-2 infection depends on cellular heparan sulfate and ACE2. Cell. 2020:183:1043–1057.
- Damus PS, Hicks M, Rosenberg RD. Anticoagulant action of heparin. *Nature*. 1973:246:355–357.
- Dhurandhare VM, Pagadala V, Ferreira A, Muynck LD, Liu J. Synthesis of 3-O-sulfated disaccharide and tetrasaccharide standards for compositional analysis of heparan sulfate. *Biochemistry*. 2020:59: 3186–3192.
- Fryer A, Huang YC, Rao G, Jacoby D, Mancilla E, Whorton R, Piantadosi CA, Kennedy T, Hoidal J. Selective O-desulfation produces nonanticoagulant heparin that retains pharmacological activity in the lung. *J Pharmacol Exp Ther*. 1991:282:208–219.
- Giavarina D. Understanding Bland Altman analysis. *Biochem Med* (Zagreb). 2015;25(2):141–151.
- Harris EN, Cabral F. Ligand binding and signaling of HARE/Stabilin-2. *Biomol Ther*. 2019:9:273–287.
- Huang Y, Mao Y, Zong C, Lin C, Boons G-J, Zaia J. Discovery of a heparan sulfate 3-O-sulfation specific pealing reaction. *Anal Chem.* 2015;87:592–600.
- Huebener P, Pradere JP, Hernandez C, Gwak GY, Caviglia JM, Mu X, Loike JD, Jenkins RE, Antoine DJ, Schwabe RF. The HMGB1/RAGE axis triggers neutrophil-mediated injury amplification following necrosis. *J Clin Invest*. 2015:125:539–550.
- Li G, Li L, Tian F, Zhang L, Xue C, Linhardt RJ. Glycosaminogly-canomics of cultured cells using a rapid and sensitive LC-MS/MS approach. ACS Chem Biol. 2015;10:1303–1310.
- Liu J, Li J, Arnold K, Pawlinski R, Key N. Using heparin molecules to manage COVID-19, Res Pract Thromb Haem. 2020:4: 518–523.
- Miller CM, Xu Y, Kudrna KM, Hass B, Kellar BM, Egger AW, Liu J, Harris EN. 3-O-sulfation of heparin leads to hepatotropism and longer circulatory half-life. *Thromb Res.* 2018:168:80–87.
- Mohamed S, Coombe DR. Heparin mimetics: their therapeutic potential. *Pharmaceuticals (Basel)*. 2017:10:78.
- Oduah EI, Linhardt RJ, Sharfstein ST. Heparin: past, present, and future. *Pharmaceuticals (Basel)*. 2016:9:38.
- Ouyang Y, Yu Y, Zhang F, Chen J, Han X, Xia K, Yao Y, Zhang Z, Linhardt RJ. Non-anticoagulant low molecular weight heparins for pharmaceutical applications. *J Med Chem.* 2019:62: 1067–1073.
- Palm M, Mattsson C. Pharmacokinetics of fragmin. A comparative study in the rabbit of its high and low affinity forms for antithrombin. *Thromb Res.* 1987:48:51–62.
- Pempe E, Xu Y, Gopalakrishnan S, Liu J, Harris EH. Probing the structural selectivity of synthetic heparin binding to the stabilin receptors. J Biol Chem. 2012;287:20774–20783.
- REMAP-CAP T, ACTIV-4a, Investigators A. Therapeutic anticoagulation with heparin in critically ill patients with COVID-19. *N Engl J Med*. 2021:385:777–789.
- Stehle G, Wunder A, Sinn H, Schrenk HH, Harenberg J, Malsch R, Maier-Borst W, Heene DL. Pharmacokinetic properties of LMW-heparin-tyramine fractions with high or low affinity to antithrombin III in the rat. *Semin Thromb Hemost*. 1997:23:31–37.
- Sundaram M, Qi Y, Shriver Z, Liu D, Zhao G, Venkataraman G, Langer R, Sasisekharan R. Rational design of low-molecular weight heparins with improved in vivo activity. *Proc Natl Acad Sci.* 2003:100: 651–656.
- Voynow JA, Zheng S, Kummarapurugu AB. Glycosaminoglycans as multifunctional anti-elastase and anti-inflammatory drugs in cystic fibrosis lung disease. *Front Pharmacol*. 2020:11:1011.
- Wang Z, Arnold K, Xu Y, Pagadala V, Su G, Myatt H, Linhardt RJ, Liu J. Developing a quantitative method to analyze heparan sulfate using isotopically labeled calibrants. Commun Biol. 2020;3(1):425.

- Wang Z, Dhurandhare VD, Mahung CA, Arnold K, Li J, Su G, Xu D, Maile R, Liu J. Improving the sensitivity for quantifying heparan sulfate from biological samples. *Anal Chem.* 2021:93:11191–11199.
- Wang Z, Arnold K, Dhurandhare VM, Xu Y, Pagadala V, Labra E, Jeske W, Fareed J, Gearing M, Liu J. Analysis of 3-O-sulfated heparan sulfate using isotopically labeled oligosaccharide calibrants. *Anal Chem.* 2022;94:2950–2957.
- Warttinger U, Giese C, Harenberg J, Holmer E, Krämer R. A fluorescent probe assay (Heparin Red) for direct detection of heparins in human plasma. *Anal Bioanal Chem.* 2016:408:8241–8251.
- Xu Y, Cai C, Chandarajoti K, Hsieh P, Lin Y, Pham TQ, Sparkenbaugh EM, Sheng J, Key NS, Pawlinski RL, et al. Homogeneous and reversible low-molecular weight heparins with reversible anticoagulant activity. Nat Chem Biol. 2014:10: 248–250.
- Xu Y, Chandarajoti K, Zhang X, Pagadala V, Dou W, Hoppensteadt DM, Sparkenbaugh E, Cooley B, Daily S, Key NS, et al. Synthetic oligosaccharides can replace animal-sourced low-molecular weight heparins. *Sci Transl Med.* 2017:9: eaan5954.